Miura-ori Origami Inspired Tessellation Array for a Reconfigurable Patch Antenna

Undergraduate Honors Thesis

Presented in Partial Fulfillment of the Requirements for Graduation with Distinction in the Department of Mechanical and Aerospace Engineering of The Ohio State University

By

Abdullahi Inshaar

Honors Undergraduate Program in Electrical Engineering

The Ohio State University

April 2019

Thesis Committee:

Ryan L. Harne, Advisor

Asimina Kiourti

ABSTRACT

Reconfigurable antennas are an emerging class of antennas that have a wide range of applications in the areas of wearable electronics and wireless communications. Previous research efforts have been focused on reconfiguration of antennas to enable changes in antenna electromagnetic (EM) wave properties such as radiation characteristics, resonant frequency and direction of propagation. Through reconfiguration of the antenna such as folding, or deformation, resonant frequency, gain, and direction of radiation can be fined tuned. To examine a new approach to concepts of the previous works, this research devises methods to yield reconfigurable antenna that deliver EM properties that are independent of configuration. Such as consistent resonant frequency, gain, and radiation despite folding and deformation. To study significant reconfiguration potential, this research explores the use of the miura-ori origami inspired tessellation array as basis for reconfigurable antennas. To overcome the technical challenges of reconfigurable antennas, this research implements design methods that allow for antennas to be deformed by utilizing flexible substrates and thin copper laminates. The reconfigurable antennas are assessed through a finite element modeling software and followed by experimental fabrication and testing. Tessellation based antennas allow for a large shape change resulting in the ability to analyze and understand how deformation effects the behavior of the antenna. The results of this research demonstrate that the tessellation-based patch antenna which provides folding capabilities and large deformation enables for electromagnetic wave characteristics that are independent of configuration.

ACKNOWLEDGEMENTS

I would like to first thank Dr. Harne for all the support and guidance that he has provided throughout my research endeavors.

I would also like to thank Dr. Kiourti for providing me with the necessary resources to conduct my research and for her contribution as my defense committee member.

I would also like to thank Chengzhe Zou and Saad Alharbi for all the help they have provided.

All related experiments in this research are conducted in the Laboratory of Sound and Vibration Research (LSVR) that is directed by Dr. Harne and the Wearable and Implantable Technologies (WIT) lab that is directed by Dr. Kiourti.

TABLE OF CONTENTS

LIST OF FIGURES

LIST OF TABLES

1 INTRODUCTION

1.1 Background on reconfigurable antennas

Antennas have a wide range of applications and use cases whether it's wireless or satellite communication. Through the transmission of electromagnetic waves or radio waves, antennas can operate to send or receive signals. There are a variety of antenna types such as the dipole, loop, helical, and patch that each enable for distinct applications. Current conventions create antennas that are rigid in shape, whether is a patch or dipole antenna. These physical characteristics which do not adhere well to changes, control the operation of the antenna. Various research efforts are focusing on reconfigurable antennas to fine tune the resonant frequency of an antenna [1] [2] [3] [4] [5] [6] [7] [8] [9] [10] [11]. Other research efforts focus on the control of the radiation pattern and directions [12] [13] [14]. Some of these designs' and their approaches can be seen in Figure 1.

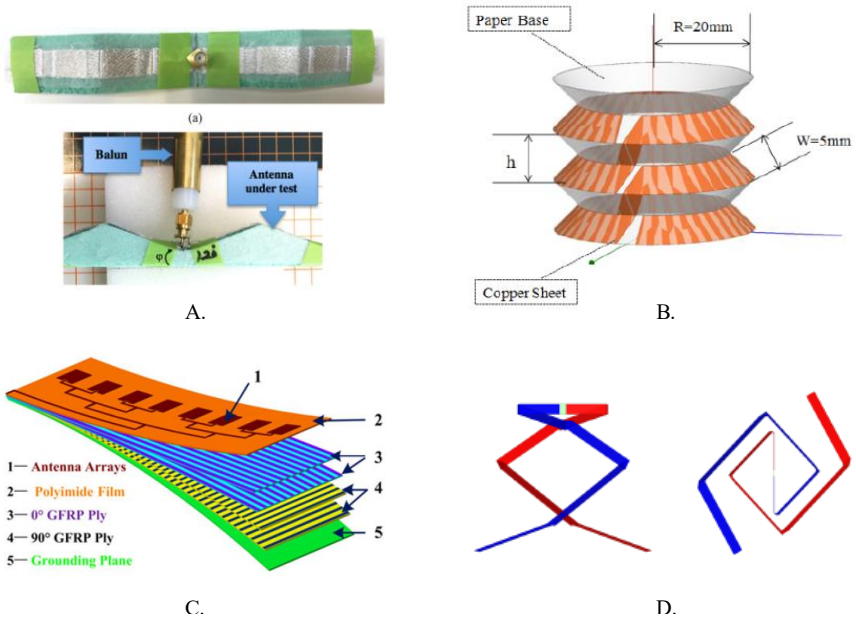

Figure 1: E-textile based dipole antenna (A) [1] and an accordion antenna (B) [4] are used to fine tune the resonant frequency through folding or change of height. A patch antenna array (C) [12] incorporated on a flexible laminate and dipole antenna (D) [14] incorporated on a Nojima origami shape are used to tune the radiation characteristics of the antenna.

Frequency shifts can be used to quantify deformation [1] [8] [11] [13] or deformation can be used to create a single antenna design that can operate over a range of frequencies [4] [9] [14]. The idea of changing radiation pattern and direction is to create adaptable antennas for emerging wireless and satellite communications that can be reconfigured relative to usage and interference as to enhance performance and coverage. Resonant frequency shifting through foldable antennas creates a way to transmit information efficiently over a wide range of parameters. Despite this, studying reconfigurable antennas that provide consistent behavior is important for applications in wearable electronics. Various electronic devices and components function and benefit from consistency and these devices can benefit for reconfigurable antennas that provide this consistent behavior. This in turn can expand the applications of wearable electronics.

Tessellation based antennas that are capable of folding provide guidance, flexibility, and adaptability for a variety of applications.

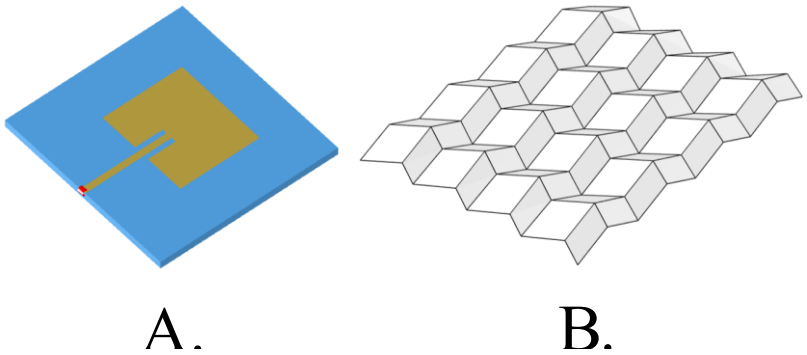

Figure 2: Typical rectangular patch antenna design (A) with a transmission line feed and a miura-ori origami tessellation (B)

So, a planar patch antenna is incorporated onto a miura-ori origami tessellation. The patch antenna when folded exbibits electromagnetic properties that are independent of folding. The development of a foldable patch antenna involves the use of a thin polypropylene substrate with the incorporation of a miura-ori tessellation. This shape creates a foldable substrate in which the copper ground plane and patch of the antenna can be incorporated on to. They exhibit large shape change relative to small changes in folding angles allowing for careful study of how folding and deformation effect the behavior of the antenna. Over the previous design methods, this array method of the tessellation-based technique can provide for robust and repeatable designs that are easily deformed, scaled, and reproduced. The planar arrays can in turn be incorporated onto surfaces such as on clothing as wearables to enable smart electronics that provide consistent behavior.

1.1 Research goal

The goal of this research is to develop a reconfigurable antenna that has electromagnetic wave characteristics that are independent of folding and deformation. This antenna can in turn be utilized in applications where surface deformation and folding occurs. By providing properties that are independent of folding this antenna can be utilized for its robust behavior. Utilizing simulation and experimental testing of tessellation-based patch antenna, folding and deformation can be induced. In turn the electromagnetic wave properties of the antenna can be studied.

1.2 Thesis overview

From modeling, fabrication, and testing various stages of the research are covered. In chapter 2 the concept of modeling the antenna using COMSOL Multiphysics is covered with an overview of how the finite element (FE) modeling is conducted, how the physics is defined, what study is run, and an analysis of results. In chapter 3, the experimental fabrication methods are covered and as well as what did and did not work. An outline of the testing methods and procedures of the antenna followed by an analysis of the results in chapter 4.

2 TESSELLATION-BASED PATCH ANTENNA MODELING

COMSOL Multiphysics is a finite element (FE) modeling software that is used to create the computational models of tessellation-based patch antennas. The computational model enables for induced folding of a patch antenna while using the Electromagnetic Waves, Frequency Domain (EMW) physics interface to provide an understanding for how the electromagnetic wave properties of the antenna change relative to folding and deformation. The following sections of this chapter show the modeling process, explain the studies conducted, explain the results obtained and explain the use case of modeling to guide experimental fabrication. The process consists of creating the geometry and defining the parameters of the antenna such as the patch, substrate, and ground plane. Incorporating an Electromagnetic Waves study allows us to compute, analyze and study various parameters of the design relative to frequency.

2.1 Finite element (FE) modeling

The miura-ori tessellation is a form of rigid origami that enables for folding of a planar sheet into to a compact shape. It is comprised of repeated facets in the shape of parallelograms. Four parallelograms make up a single miura-ori unit [15]. As shown in Figure 3 by defining mountains and valleys, the folding capabilities of the miura-ori can be established. This shaped enables for folding that can be induced by parallel inputted forces from the two flat sides of the tessellation.

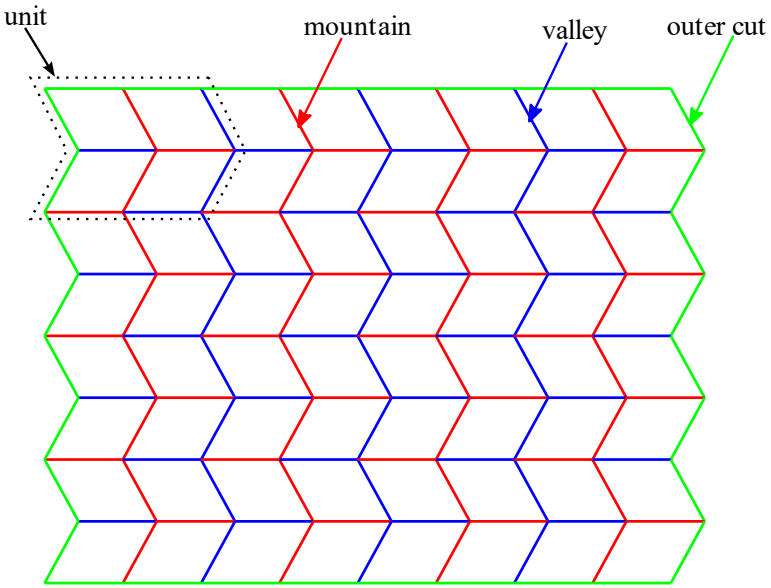

Figure 3: Miura-ori tessellation pattern, usually a single unit (2x2) is created and this pattern can be repeated to generate a full tessellation.

A typical rectangular patch antenna with the use of a recessed micro-strip transmission line is shown in Figure 4 (A and B). The geometry of the patch antenna is made up of four main components, the ground plane, substrate patch and transmission line. These geometrical entities as shown in Figure 4 are defined in the COMSOL model as domains or boundaries.

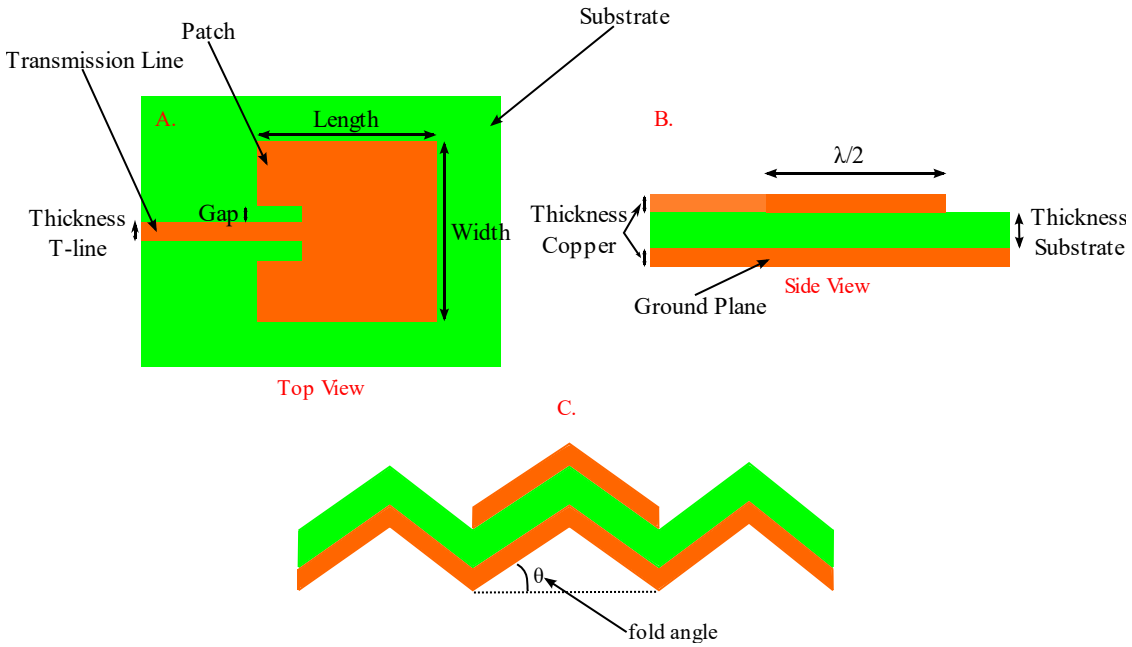

Figure 4: Typical patch antenna design (A and B) with the implementation of a folding characteristic (C)

A geometrical domain in the shape of the tessellation is defined as the substrate of the antenna. The ground plane, patch and transmission line are defined as boundaries. The domains have a certain thickness which in this case is defined as the thickness of the substrate. The boundaries are just surfaces with no thickness which saves on computational cost such as time and memory. The ground plane, transmission line and patch consist of copper while the substrate is air. Figure 5 showcases the modeling specifications relative to the patch antenna incorporated onto a miura-ori tessellation. There are several parameters that control the miura-ori tessellation, but the few of interest at the fold angle, length, width, height, thickness of the transmission line and the induced frequency. The lumped port is used to connect the transmission line to the ground plane and is where the excitation of the antenna occurs. By controlling the fold angle (θ), how folding effects the antenna behavior can be studied.

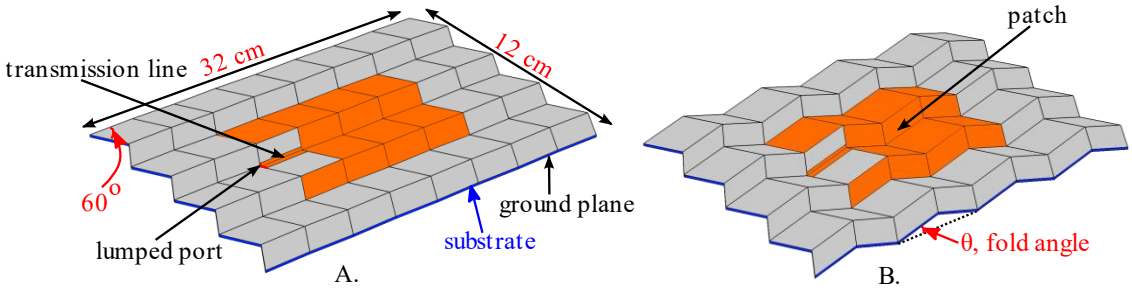

Figure 5: Miura-ori tessellation geometry as defined in COMSOL with the incorporation of a patch antenna capable of folding for a given angle theta

For the model to demonstrate testing of the antenna in an anechoic test chamber, a perfectly matched layer (PML) in Figure 6 A is used to minimize reflections of waves that pass-through modeling domain (far field

domain). The modeling domain defines the region of interest which is set as the boundary of the far field domain. So, any RF waves that pass through the far filed domain will be perfectly absorbed by a perfectly matched PML. The antenna sits in the middle of this spherical domain.

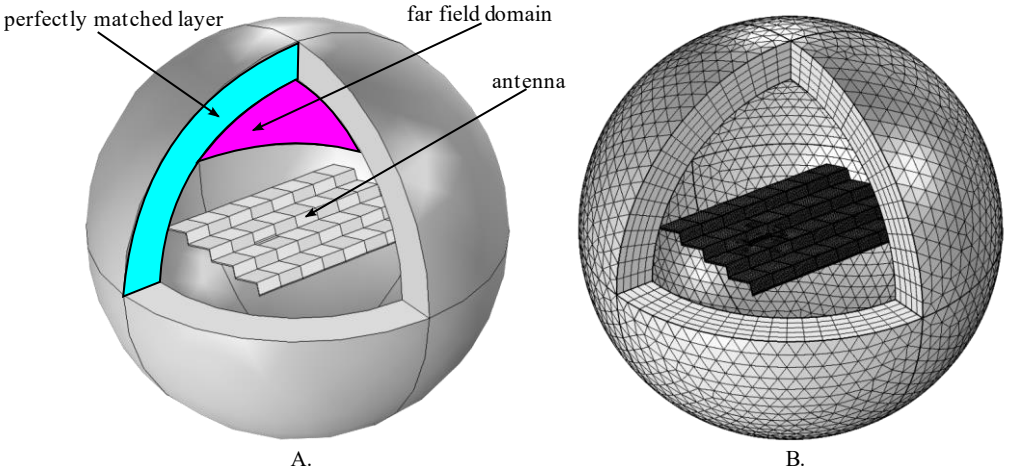

Figure 6: 3D visualization of the COMSOL model which can demonstrate testing of the antenna in an anechoic test chamber

The mesh in Figure 6 B is a physics-controlled mesh in which the maximum mesh element size is determined by the minimum wavelength in a vacuum as shown in Equation 1. Where "c" is the speed of light in a vacuum and "f" is the operating frequency. The value of "f" can be selected depending on the highest frequency range of the study. If the computational resources permit, "f" can be chosen higher to ensure a well-defined mesh for the study.

$$\lambda = \frac{c}{f} \tag{1}$$

The Electromagnetic Waves, Frequency Domain (EMW) is used to solve for time-harmonic electromagnetic field distributions. The Frequency Domain analysis is used for the analysis of the source driven models such as the patch antenna across a range of frequencies. This physics interface has a variety of subset nodes that are automatically generated such as Wave Equation: Electric, Perfect Electric Conductor, Initial Values, Lumped Port, and Far-Field Domain. The Wave Equation: Electric, is the main governing node which applies to all domain in the model. The Perfect Electric Conductor is used to define the lossless metallic boundaries within the model which include the patch, transmission line and ground plane. The Initial Values sets an initial electric field distribution **E** in V/m in the model which is comprised of an x, y, and z component which can be initialized separately. For the model, the initial x, y, and z components are set to zero. The lumped port is used as the excitation port of the antenna. The port is defined between the transmission line and the ground plane which are two conductive boundaries. This port acts as the wave excitation port with an induced voltage V_o of 1 V and a characteristic impedance Z_{eff} of 50 Ω. The definition of the Far Field Domain enables variables such as far field gain, norm, and far field variable x, y, and z which can be plotted after the simulation.

2.2 S_{11} vs frequency results

A Parametric Sweep and Frequency Domain are utilized to define desired fold angles and the frequency range with a value range for each. The fold angles can be defined in terms of degrees. The frequency range which is defined in terms of Hz. For the model specifications, the fold angle has set boundaries of 0 to 90 degrees. The frequency range is a sweep that is defined relative to the approximate operating frequency of the antenna f_o. This operating frequency can be determined as defined in Equation 2**.**

$$f_o = \frac{1}{2L\sqrt{\mu\varepsilon}} = \frac{c}{2L\sqrt{\varepsilon}} \tag{2}$$

Where "L" is the length of the patch antenna in meters, "μ" is the permeability of free space in H/m, "ε" is the relative permittivity value of the dielectric substrate in F/m, and "c" is the speed of light in m/s. Dielectric materials which comprise the substrate of the patch have a permittivity value "ε_r". Vacuums have the lowest possible permittivity value of $8.85\text{x}10^{-12}$ F/m which is defined as "ε_o". The relative permittivity is defined in Equation 3.

$$\varepsilon = \varepsilon_r \varepsilon_o \tag{3}$$

For the model, the substrate consists of air which in the model is a perfect vacuum. The relative permittivity of the substrate is $8.85\text{x}10^{-12}$ F/m. The length of the patch antenna is defined as 0.16 m. Using Equation 2, the approximate resonant frequency (f_o) is calculated as 0.94 GHz. A frequency sweep from 0.9 to 1 GHz with 100 data points is defined and the fold angles are defined as 1º, 20º, 40º, and 60º. The resulting plot in Figure 7 is obtained after running the simulation for the set angle values and frequency range.

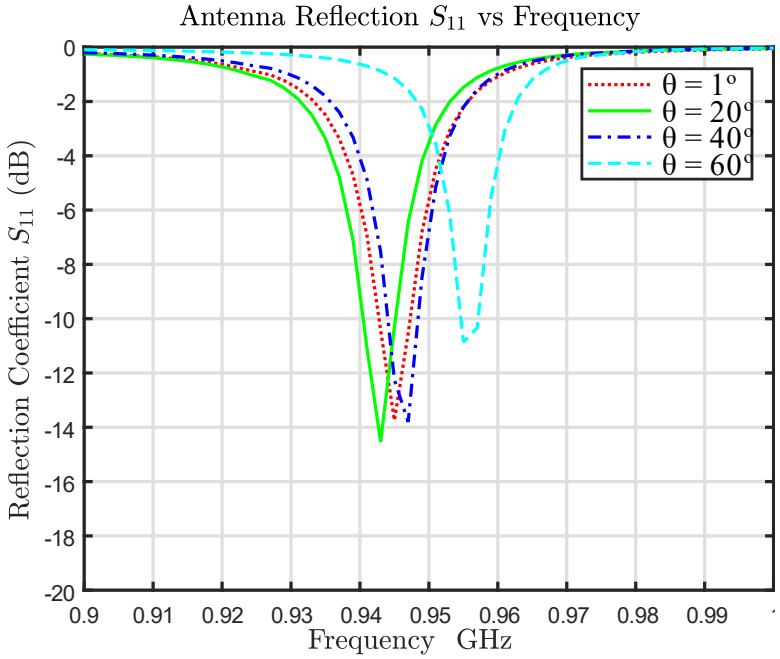

Figure 7: Simulation results for the frequency of operation and return power loss of the antenna relative to folding, the approximate calculated f_o (0.94 GHz) matches closely with that of the simulation

The plot indicates the return loss (S_{11}) at each specific frequency. The lower S_{11} values indicate that the antenna is effective at transmitting the input power. The effective S_{11} vs frequency plot showcases how induced folding effects the frequency of operation of the antenna and its bandwidth. There is minimal shifting in the resonant frequency at θ values less than 40°. The bandwidth of the antenna remains consistent at the different fold angles. The S_{11} at the resonant frequency indicates that that the antenna is effective in transmitting input power.

Fold angle θ (deg)	Resonant frequency fo (GHz)	Percent variation (%)
1	0.9449	+0.00
20	0.9429	-0.20
40	0.9469	+0.20
60	0.9551	+1.02

Table 1: Resonant frequency shift analysis as a percent variation of f_0 for specified fold angles. The shift is relative to f_0 at 1-degree fold and the range is defined as the 1 GHz which is the frequency range of the sweep.

The resonant frequency shift variation as a percentage value relative to the initial resonant frequency at 1-degree fold in Table 1 indicates that folding has very minimal effects of the resonant frequency of the antenna. For fold angles of 40° or less a shift of 0.2% is achieved. The low S_{11} values at the resonant frequencies for the 1°, 20°, and 40° fold angles indicates that the antenna remains consistent in transmitting input power. The target value of the resonant frequency at 60° was not hit in the simulation, however it can be approximated to fall within the range of -12 to -14 dB.

2.3 Electric distribution and gain results

The surface electric field norm distributions, and 3D far field gains are used to study how the folding of the antenna effects its overall behavior. From the front edge to the back edge, the voltage, current, and impedance distributions follow wave like patterns across the resonant length of the antenna as shown in Figure 8. With the interest of analyzing the first resonant frequency the wave corresponds to half the wavelength.

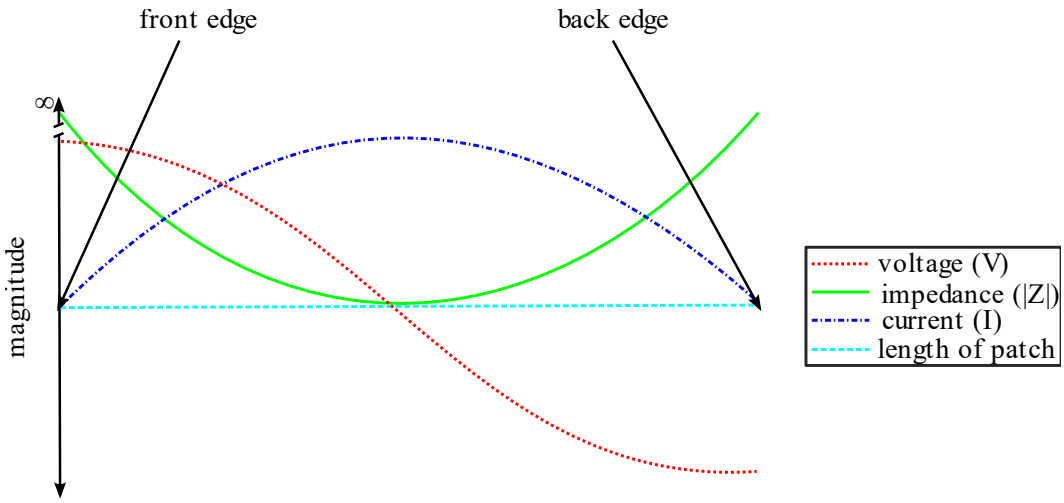

Figure 8: Voltage, current, and impedance distribution over the length of a patch antenna where the front edge corresponds to the edge in which transmission line is fed from

Four folding angles are simulated in these cases, 1°, 20°, 40°, and 60°. Figure 9 A through D, showcase how the voltage is distributed over the length of the patch. The voltage distribution follows that half wavelength pattern as previously indicated. The high-density areas (front and back edge) correspond to the edges at which the patch radiates from. The front edge tends to have a higher voltage distribution than that of the back as seen by the darker red color due to the front edge having only two facets while the back edge had four facets. There is a conservation of power that occurs at the front resulting in a higher voltage distribution per facet.

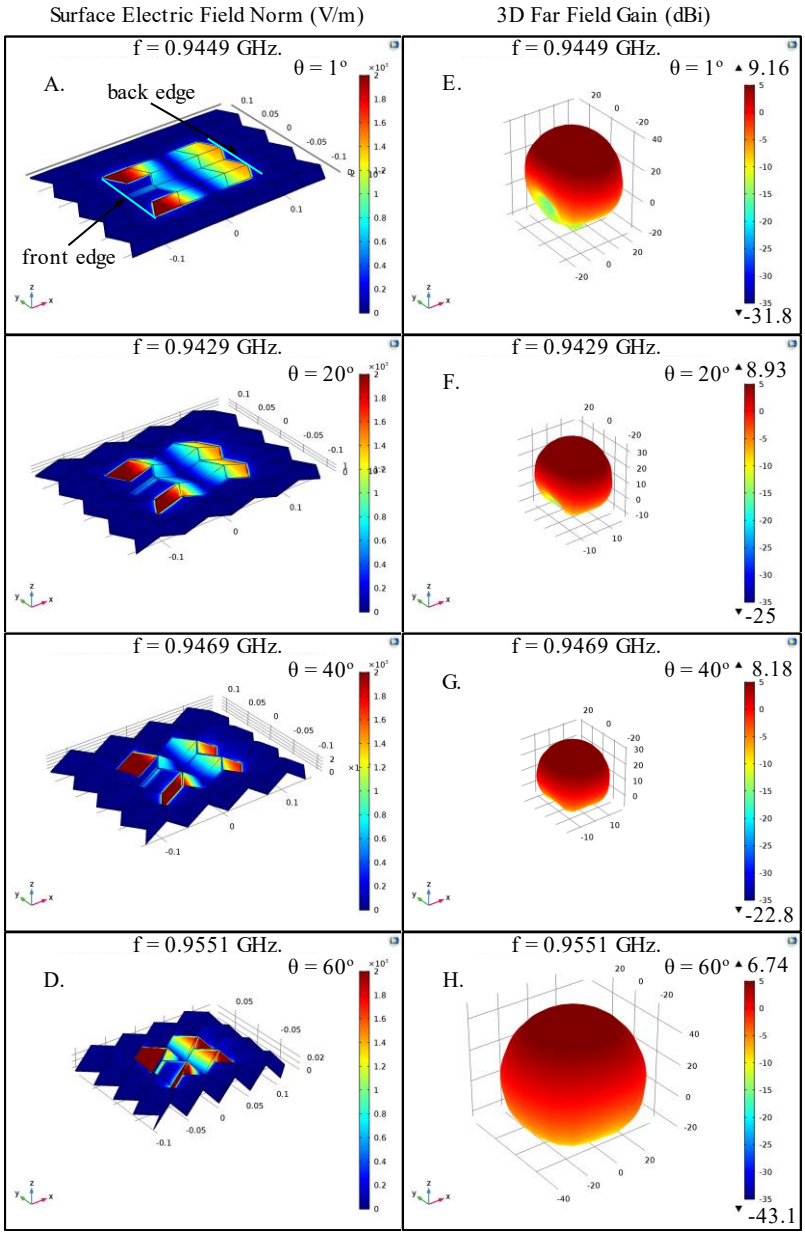

Figure 9: Simulation results for the surface electric field distribution (V/m) and the 3D far field gain (dBi) of the antenna

Figure 9 E through F showcase the radiation pattern, radiation direction, and gain of the antenna. Like the typical patch antenna, the radiation occurs in the direction that is perpendicular to the surface of the patch. In this case, the antenna always radiates in the positive z-direction. With folding, the antenna exhibits relatively the same behavior and gives an adequate gain in order to be able to radiate power efficiently.

Fold angle θ (deg)	Far field gain (dBi)	Difference
1	9.16	0.00
20	8.93	-0.23
40	8.18	-0.98
60	6.74	-2.42

Table 2: Far field gain difference at the various fold angles, the difference is determined by variation from the far filed gain at 1-degree fold.

For fold angles 20^{o} and 40^{o}, the fair field gain is relatively the same as that of 1^{o}. However, the gain difference at 60^{o} is quite different and this is due to the actual resonant frequency at 60^{o} not being evaluated. This can indicate that the gain at 60^{o} is higher. Radiation direction of the antenna remains consistent at the various fold angles. However, as the fold angle increases the broadside radiation increases as well. This results in a decrease in the far field domain (radiation distance) in the positive z-direction as the radiation increases in the positive x and y-directions. The fringe field lines as shown in Figure 10 showcase that as the fold is increased the fringing field lines increase their radial distance in the x-direction. Which in turn creates a greater broadside radiation in the x-direction. The side edges do not radiate so there is minimal variation in the 3D far field gain relative to the y-direction.

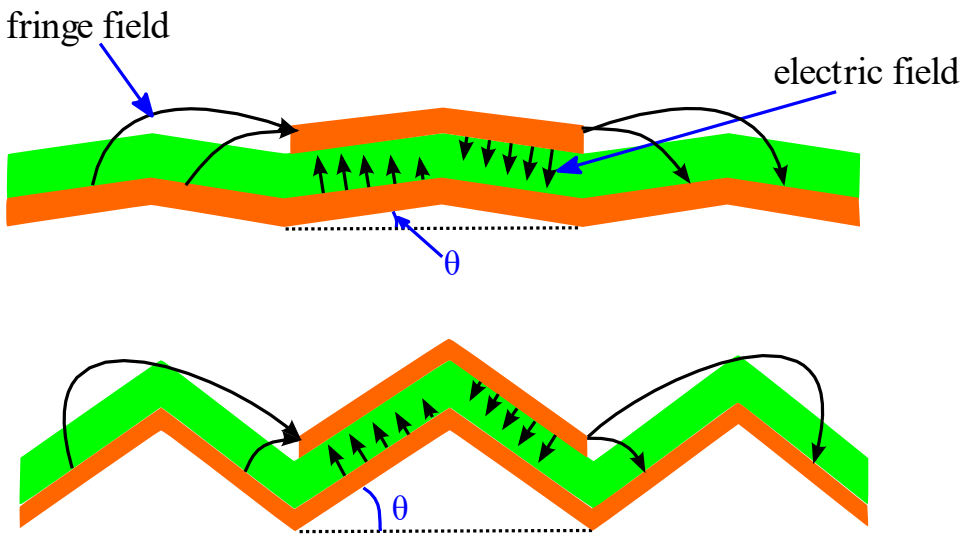

Figure 10: Electric and fringe field lines relative to fold angle. The fringe lines which are produced at the front a back side of the antenna relative to the feed point are what cause the antenna radiation.

3 EXPERIMENTAL METHODS

Miura-ori tessellation-based patch antennas must be designed in order to analyze how induced folding and deformation effect the electromagnetic properties of the antenna. The developed designs need to be able to fold and create large shape change of the antenna. Section 3.1 covers modifications that are made to the model in order to achieve a model that can tested. So, two fabrication methods are covered as well as their feasibilities for foldable miura-ori tessellation-based antennas. Section 3.2 and 3.3 cover the experimental setup involving the use of a Network Analyzer, and RFExpert, and testing to see how electromagnetic properties of the antenna are affected relative to folding.

3.1 Antenna design and fabrication

The COMSOL model has a transmission line which ends towards the center on the miura-ori tessellation. While this was ok for the modeling purpose, the transmission line needs to be extend towards the front edge so that a SMA connector can be connected for experimental testing.

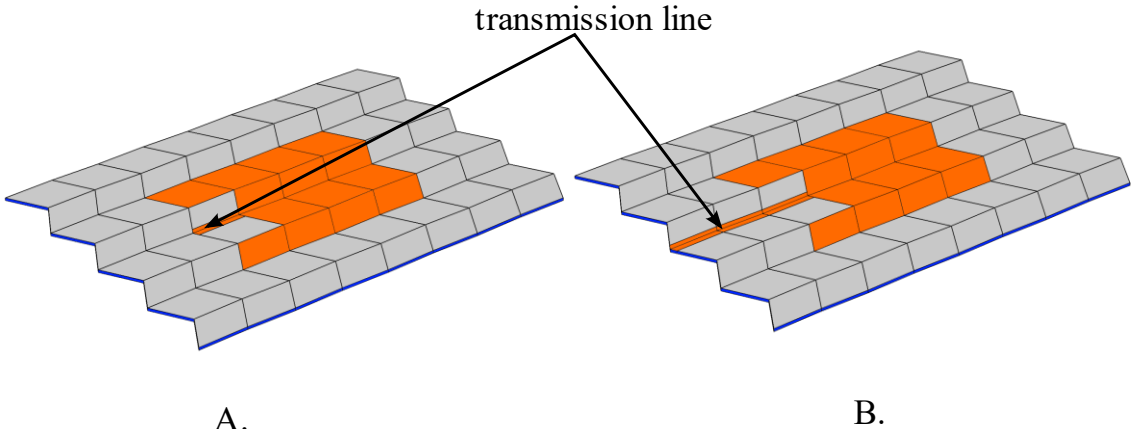

Figure 11: The simulation model (A) is slightly updated (B) so that the transmission line is the at front edge of the miura-ori tessellation. This allows for the connection of the SMA connector in the fabrication process.

Using Advanced Design System (ADS) software a 2-D model of the antenna is developed. This model is then used to extend the transmission line to the front edge of the tessellation. The width of the transmission line is determined using the available transmission line matching tools such as LineCalc in ADS.

Initially fabrication of the antennas involved the use of a CNC router as shown in Figure 12 A. High frequency copper laminates RT/duroid 5870NS and 5880LZ were utilized in the fabrication process. These laminates consist of a two thin copper layers and a glass microfiber reinforced Polytetrafluoroethylene (PTFE) composite as the substrate.

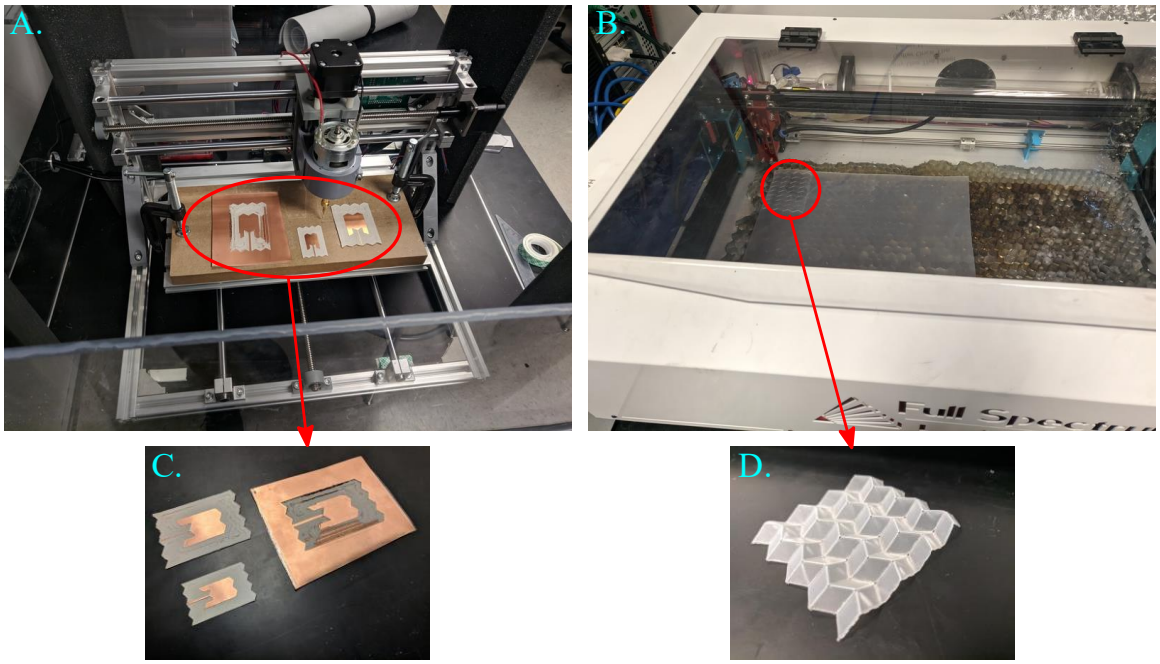

Figure 12: The initial fabrication method using RT/duroid laminates is shown in A with some of the resulting antennas in C. The second fabrication method using a laser cutter is shown in B with the resulting miura-ori tessellation based polypropylene substrate in D.

Laminate	Thickness of copper foil (µm)	Thickness of substrate (µm)	Dielectric constant ε_r	Dissipation factor tan δ
5870NS	18	254	2.33	0.0005- 0.0012
5880LZ	18	508	2.00	0.0021

Table 3: Electrical properties of the RT/duroid laminates.

This fabrication process involved first milling the top layer of the copper and second cutting out the outer edges as shown in Figure 12 C. While these laminates provide excellent electrical characteristics such as uniform dielectric constants and low dissipation factors, they do not adhere to folding very well. With very minor folding, the extremely thin copper foil tends to crack. This isn't acceptable in the design as the thin transmission line will tend to crack, creating a discontinuity which impedes the excitation of the antenna.

The second fabrication method as shown in Figure 12 B, involved the use of thin flat polypropylene sheets that were engraved and cut to form the substrate of the antenna.

Laminate	Thickness of copper foil (μm)	Thickness of substrate (μm)	Dielectric constant ε_r	Dissipation factor tan δ
Custom: copper foil and polypropylene	25	508	2.3	0.0003-0.0005

Table 4: Electrical properties of the custom laminates using a polypropylene substrate [16] and copper foil.

This design provides the substrate of the antenna that can be folded as shown in Figure 12 D. Initially, the vector maps shown in Figure 13 are created in Inkscape. The three geometries that are created are the ground plane, substrate and patch with transmission line. Starting off with the substrate, the vector lines in Figure 10 A are utilized by the laser cutter. The red and blue lines which correspond to the mountains and valleys of the tessellation are laser engraved on the polypropylene material. The outer green line is the final shape that is cut out by the laser. The copper laminates consist of a thin copper layer, followed by a thin layer of adhesive and finally a sheet of paper as the backing. The laser cannot cut the ground plane and patch which consist of copper. So, the paper on the backing of the copper laminates is utilized as a canvas. The shape of ground plane and patch are drawn on the paper using the laser and then cut out by hand.

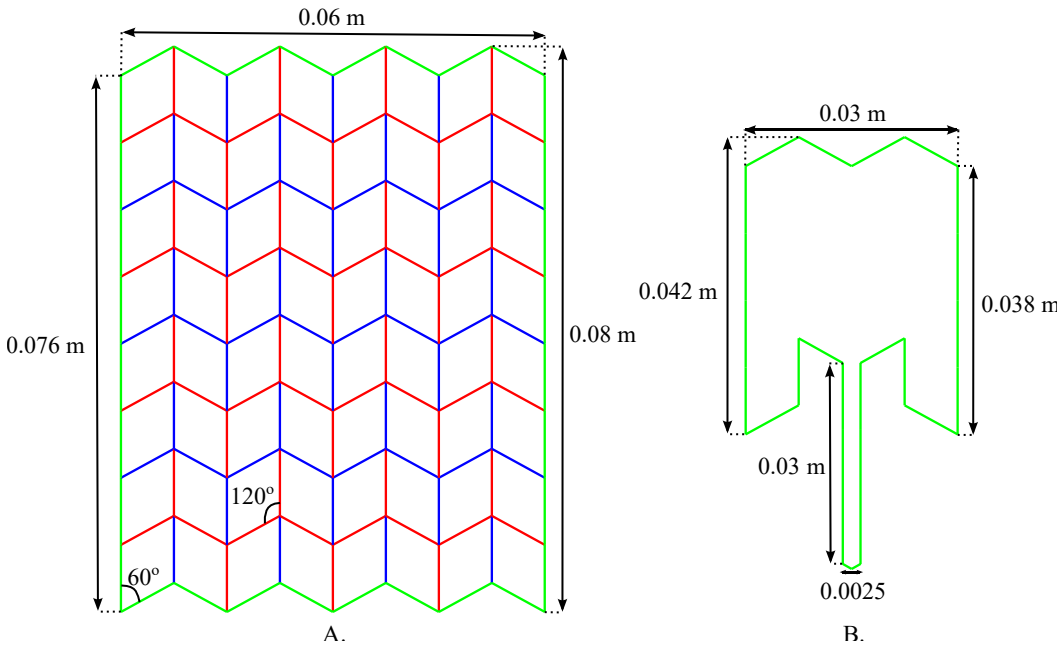

Figure 13: Vector lines for the ground plane, patch with the transmission line and substrate which are utilized by the laser cutter to create the corresponding miura-ori shapes. A showcases the vector lines for the substrate. B showcases the vector lines for the patch with transmission line. The outer green outline in A corresponds to the vector lines utilized as the shape of the ground plane.

In order to analyze how folding effects, the EM properties of the antenna, a control antenna corresponding to a fold angle of 0° is first created as shown in Figure 14 (A). This is achieved by taking the fabricated flat polypropylene substrate and letting it remain flat. The laser cut, and hand cut shapes are combined to form

the antenna. Then using the adhesive side of the copper ground plane, the shape is overlaid on the bottom side of the polypropylene substrate. Likewise, using the adhesive side of the copper patch with transmission line cut is overlaid on the top side of the polypropylene substrate. As for the antennas that should be able to fold, the flat polypropylene material folding corresponding to the mountains and valleys is done by hand. This enables for the substrate to take on the origami shape and further folding can be easily induced after this process. The ground plane, and patch with the transmission line are overlaid on the top and bottom of the tessellation-based substrate as shown in Figure 14. Two of these pre-folded antennas that enable for further folding are shown in Figure 14 (B and C).

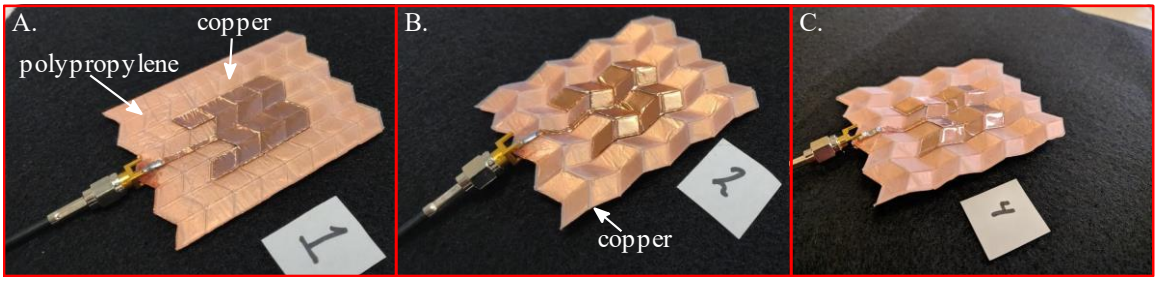

Figure 14: The three final antenna designs which all have the same physical and electrical characters. Antenna 1 (A), always remains flat. Antennas 2 and 4 (B and C) are folded to various angles.

The three antennas in Figure 14 have the same physical and electrical characteristics expect for the fold angle (θ). This allows for the study of how the folding effects the operation and EM properties of the antenna.

3.2 Experimental setup

Two methods of experimental testing are conducted to test the resonant frequency, radiation pattern, radiation direction, efficiency, and gain of the antenna at various fold angles. Figure 15 A showcases the setup using a Network Analyzer (NA) to determine the resonant frequency of the antenna and measure the return loss of the antenna. The setup involves the use of a single port, so initially a one port calibration is done. The NA can measure all the s-parameters but the one of interest is S_{11}. Figure 15 B showcases the setup using the NA in conjunction with the RFExpert to study the radiation pattern and direction as well as the gain and efficiency of the antenna. The orientation of the antenna is flipped so that the ground plane is at the top while the patch as at the bottom. To reduce coupling between the antenna and surface of the RFExpert a Styrofoam block with a height of 25 mm is used create spacing to reduce coupling. The RFExpert uses near-field electromagnetic wave measurements to evaluate and display far-field EM patterns. The measurements of interest are the 3D and 2D fair field gains.

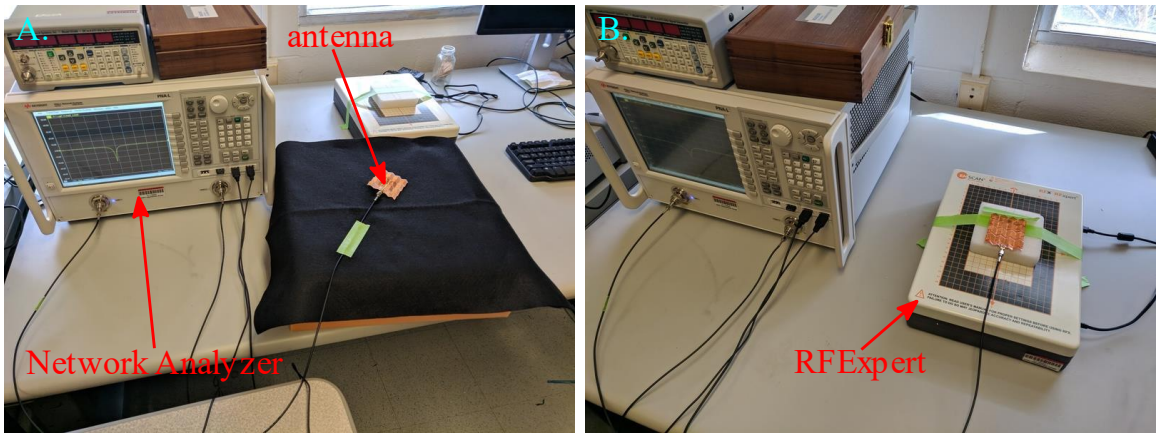

Figure 15: Shown are the two testing methods that were conducted of the antenna. A showcases the setup with the Network Analyzer while B showcases the addition of the RFExpert.

3.3 Experimental testing

To determine the approximate operating frequency of the antenna, Equation 2 in section 2.2 and the patch measurements in Figure 10 in section 3.1 and the electrical properties of the polypropylene substrate in Table 4 in section 3.1 are used. The operating frequency f_o is calculated as 2.60 GHz. The frequency sweep for the NA is set from 2.5 to 3.5 GHz with 6401 data points in between. The power is set to 5 dBm across this frequency range. Due to power loss across the cable connecting the port 1 to the antenna and variably in the actual power provided by the NA, the use of a power profile by the RFExpert is necessary. In the RFExpert software, the frequency range for the power profile is set as 2.5 to 3.5 GHz with 100 data points. To create this power profile a power meter is utilized to measure the input power across the cable at each frequency step and the RFExpert program stores the power reading for that specific frequency. The program runs through all 100 frequency points and creates the power profile. In the RFExpert program a swept frequency scan across 2.5 to 3.5 GHz with 100 data points just like the power profile is established. Then simulating over this span, the program utilizes the power profile power readings to determine the incoming power to measure the EM properties of the antenna such as far-field gain, S_{11} parameters, and efficiency.

The three antenna designs antenna 1, 2, and 4 are tested. Antenna 1 remains flat while 2 and 4 were folded relative to an approximate desired fold angle. For each testing case A through G in Figure 16, a swept frequency scan is conducted, and the EM properties are measured.

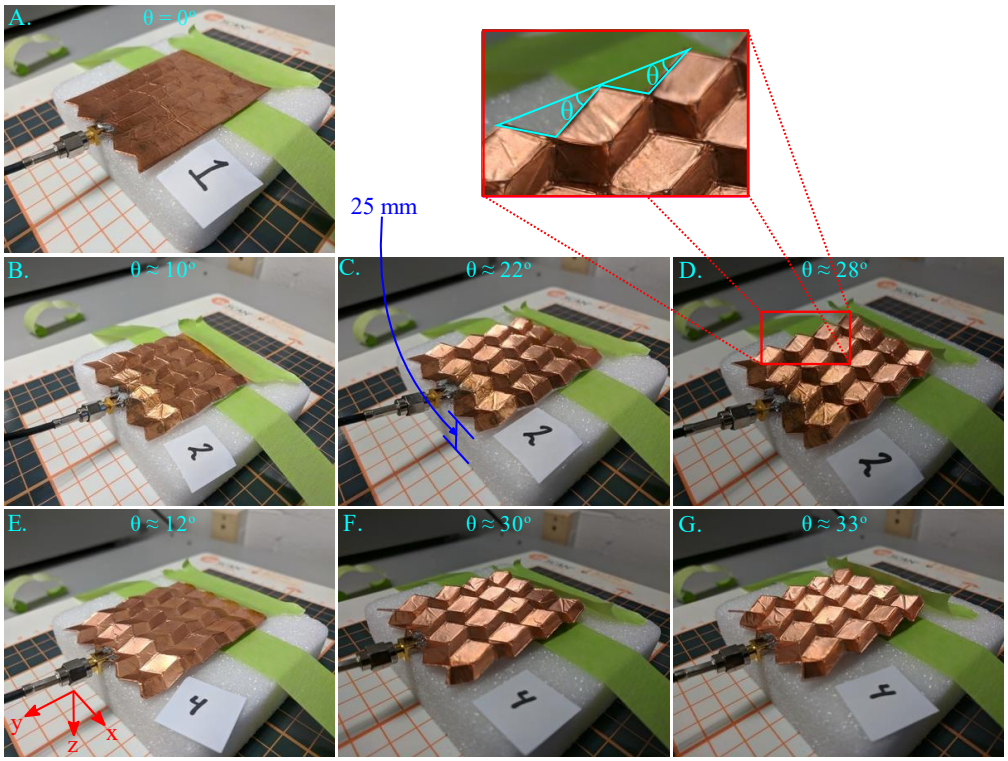

Figure 16: Different folding angles are tested using the RFExpert. A showcases testing of antenna 1. B, C, and D showcase testing of antenna 2 at different fold angles. E, F, and G showcase testing of antenna 4 at different fold angles.

When testing the antennas, specific fold angles cannot be specified. So, the fold angle is governed by qualitative measurements as partially folded, slightly folded, and mostly folded. By taking the images, the approximate fold angle θ can be approximated using Inkscape as shown in Figure 16 D.

4 RESULTS AND DISCUSSION

The goal of this research is to study how folding and deformation effects the electromagnetic properties of the patch antenna. Three antennas were fabricated on a miura-ori tessellation pattern to induce folding as well as large deformation. The antennas consisted of the same physical and electrical characteristics. Antenna 1 always remained flat while antenna 2 and 4 were capable off folding. The antennas were tested using a Network Analyzer in conjunction with an RFExpert. The following chapter showcases the obtained experimental results and provides a discussion of these results. In section 4.1 the S_{11} parameter, gain and efficiency of the antennas at various fold angles is discussed. In section 4.2 the 3D and 2D far field gain radiation pattern results are discussed.

4.1 Antenna S_{11}, gain and efficiency

The S_{11} parameters, gain, and efficiency of the antenna are some of the relations that are analyzed to see how the antenna performance changes relative to folding. The resonant frequency of the antenna, gain and efficiency collected either from the Network Analyzer of the RFExpert are analyzed. Both the Network Analyzer and the RFExpert have the same frequency range. However, the RFExpert has fewer data points do to the reliance of a stored power profile over 100 frequency points. Figure 17 A and B show the resonant frequency of the antenna at the various fold angles. The frequency shift of the antennas is very negligible as they all operate around 2.9 GHz.

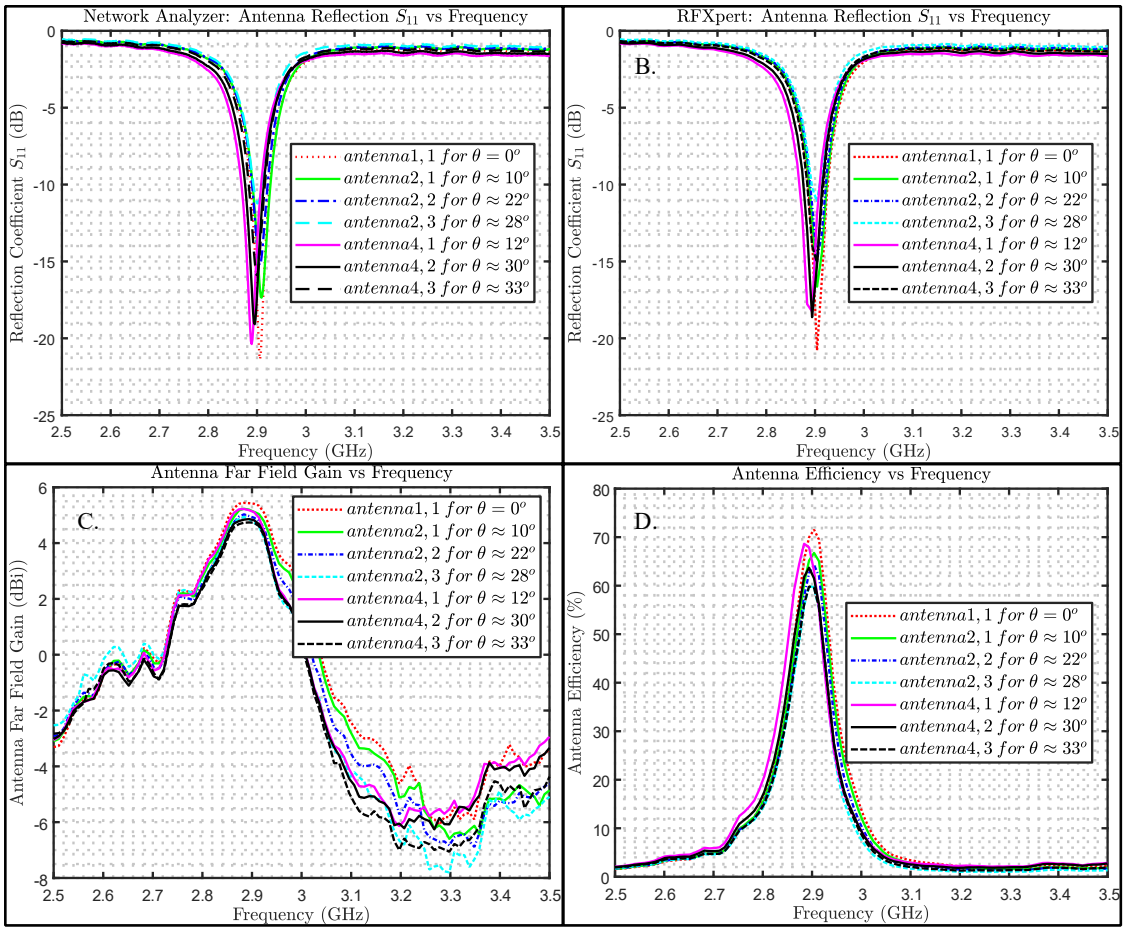

Figure 17: A and B showcase the antenna operating frequency at various fold angles collected from the Network Analyzer and the RFExpert. C showcases the gain of the antenna while D showcases the efficiency of the antenna at various fold angles.

To analyze the bandwidth of the antenna, the voltage standing wave ratio (VSWR) is determined. This ratio is a function of the reflection coefficient "Γ" in terms of magnitude. To determine the VSWR Equation 3 is utilized. The reflection coefficient data collected from the Network Analyzer is utilized to determine the VSWR.

$$VSWR = \frac{1 + |\Gamma|}{1 - |\Gamma|} \tag{3}$$

The resulting VSWR plot in Figure 18 is generated after solving for the Equation 3 for the respective S_{11} values from the antenna reflection S11 on the Network Analyzer.

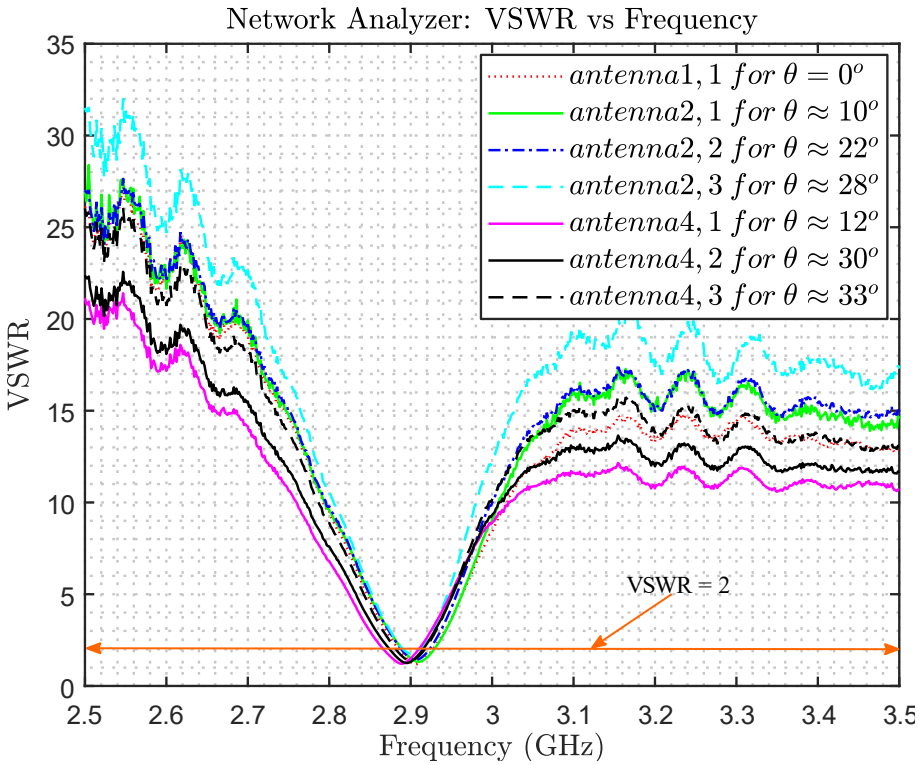

Figure 18: VSWR vs frequency with a label at VSWR = 2 to determine what the bandwidth of the antennas are at different fold angles

To look at how the bandwidth is changing relative to folding the VSWR range is set to 2. The bandwidth is determined for each fold angles by taking the two frequency values (left and right of the operating frequency) where the VSWR < 2. For example, antenna 4, 1 for $\theta \approx 12^o$, the two frequency values are 2.867 and 2.909 with a resulting bandwidth of 42 MHz. Antenna 2, 1 for $\theta \approx 12^o$, has the smallest bandwidth due to having greater reflected power at the resonant frequency (high S_{11}) compared to the other tests. This in turn creates the smaller bandwidth. This could have been caused by a few factors that tend to change how to the antenna is operating such as orientation the antenna and the coax cable. However, the overall bandwidth of the antennas remains consistent with the slight variations being directly correlated to the magnitude of the S_{11} at the resonant frequency.

Antenna	Fold angle θ (deg)	Resonant frequency f_o (GHz)	Refection coefficient S11 (dB)	Percent variation (%)	Bandwidth (MHz)
1	0	2.906	-21.36	0.00	41
2	10	2.909	-17.36	0.30	37
2	22	2.906	-15.25	0.00	33
2	28	2.902	-11.23	-0.40	19
4	12	2.889	-20.38	-1.70	42
4	30	2.895	-19.08	-1.10	39
4	33	2.900	-15.93	-0.60	34

Table 5: Experimental S_{11} parameter and VSWR analysis for the percent variation in resonant frequency relative to antenna 1 with a fold angle 0^o and the bandwidth of the antennas.

Figure 17 C shows the gain of the antenna in dBi at the various fold angles. This is a measure of the maximum power that is radiated by the antenna over an isotropic spherical domain per frequency point. At the approximate resonant frequency of 2.9 GHz the antenna gain for all the fold cases falls around 5dBi. While this shows that the antenna is pretty good at transmitting power , it shows that folding has very minimal effect on the gain. Figure 17 D shows the efficiency of the antenna. At the approximate resonant frequency of 2.9 GHz for the various fold angles, the antenna operates relatively the same. The efficiency which ranges from 60 to 70 % while low for a patch antenna it remains consistent. The RFExpert does not accept negative gain readings. Given that there are some indicated negative gain values in Figure 17 C, the RFExpert will showcase a lower than expected efficiency and gain values. Issues with the efficiency of the antenna persisted from power issues with the RFExpert so the efficiency values are lower than expected because of the RFExpert interpreting lower power values than then what was sent by the network analyzer.

4.2 3D and 2D far field gain

The 3D far field gain indicates the amount of power transmitted by the antenna and the directions at which this power is radiated towards. The gain is measured in terms of dBi which the dB measurement is over the isotropic spherical domain is. For the various fold angles, Figure 19 A through G indicate how the antenna radiates and the relative gain. The radiation beam pattern and direction of the antenna remains very consistent despite folding.

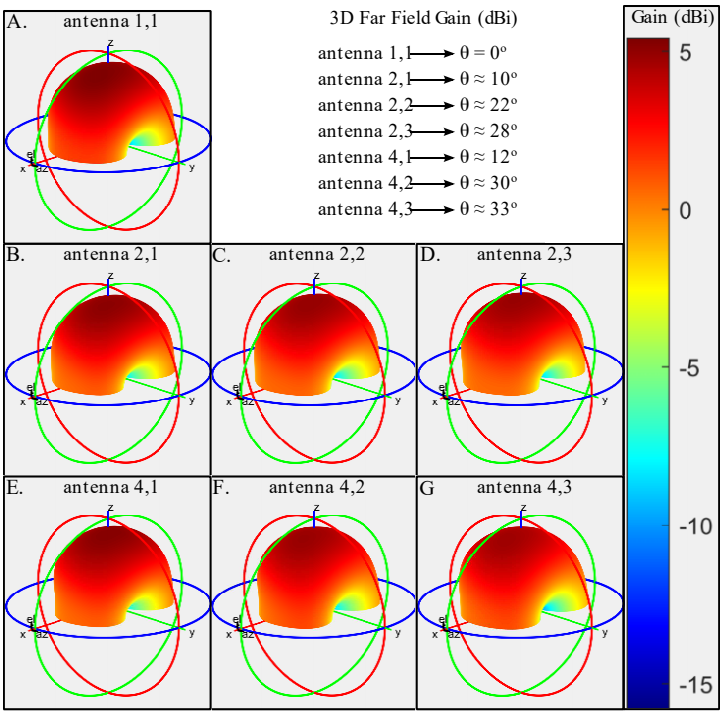

Figure 19: 3D far field gain for the antennas at the various fold angles.

Bi-section cuts are taken of the radiation beam pattern at specific angles. Figure 20 A indicates a bi-section cut taken a 0° which is a cut parallel to the xy-plane. Figure 20 B indicates a bi-section cut taken at 90° which is a cut parallel to the xz-plane. Both bi-section plots show the gain of the antenna at the specific range. They indicate that the antenna radiation direction and gain for the various regions remain relatively consistent.

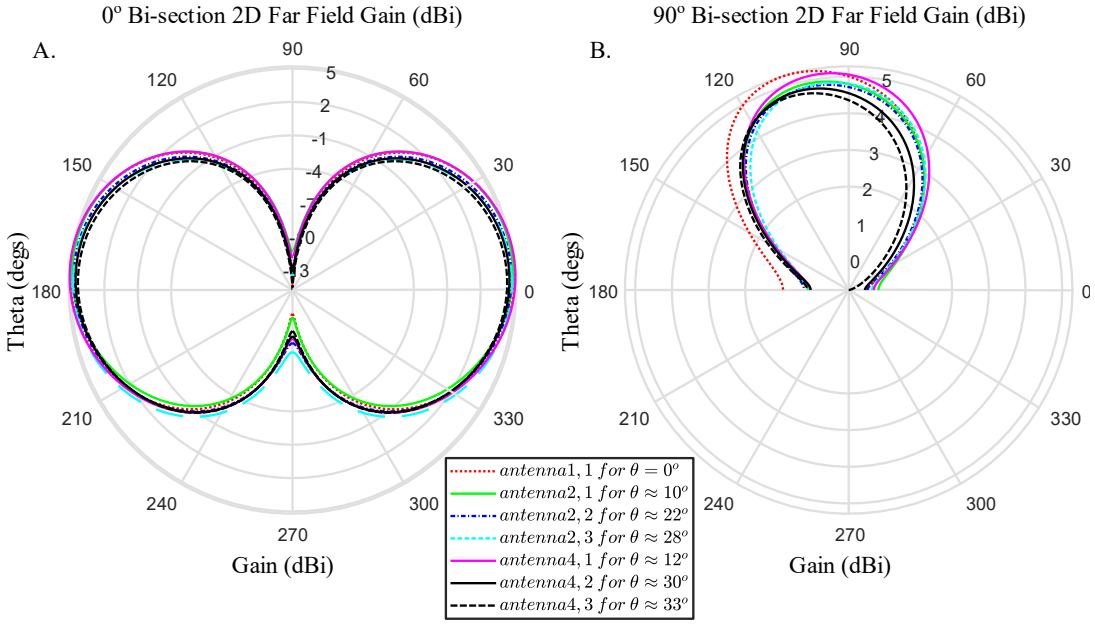

Figure 20: 2D far field gain results for the various fold angles.

5 CONCLUSIONS

There are an abundant applications in which antennas are used. Their use cases will further increase so their adaptability must as well. While antennas that can change their electromagnetic wave properties such as resonant frequency or direction of radiation offer an extra depth as to the capabilities of the antenna. Such as conveying information in the form resonant frequency shifting or having multiple modes of operation depending on deformation. There is a use case for antennas that can offer robust performance despite deformation. Various electronic devices and components function and benefit from consistency and these devices can benefit for reconfigurable antennas that provide this consistent behavior. It is found that the miura-ori based patch antenna provides robust performance relative to folding and deformation by providing consistent electromagnetic properties despite deformation. This is important in the incorporation of the designs onto wearables to provide consistent behavior over a wide range of physical deformations. Therefore, useful in applications where unchanging radiation pattern, direction, and operating frequency are necessary such as, wearables sensors, scanners and tags.

6 BIBLIOGRAPHY

[1] S. Alharbi, S. Chaudhari, A. Inshaar, H. Shah, C. Zou, R. Harne and A. Kiourti, "E-Textile Origami Dipole Antennas With Graded," *IEEE ANTENNAS AND WIRELESS PROPAGATION LETTERS,*, vol. 17, no. 12, pp. 2218-2222, 2018.

[2] K. Fuchi, G. Bazzan, A. S. Gillman, R. P. Buskohl, E. J. Alyanak and G. Huff, "Tuning Mechanisms in a Corrugated Origami Frequency Selective Surface," in *IEEE AP-S Symposium on Antennas and Propagation and USNC-URSI Radio Science Meeting*, San Diego, California, 2017.

[3] K. Fuchi, P. R. Buskohl, J. J. Joo, G. W. Reich and R. A. Vaia, "RESONANCE TUNING OF RF DEVICES THROUGH ORIGAMI," in *20th International Conference on Composite Materials*, Copenhagen, 2015.

[4] S. Yao, X. Liu, S. Georgakopoulos and M. Tentzeris, "A novel tunable origami accordion antenna," *2014 IEEE Antennas and Propagation Society International Symposium (APSURSI)*, pp. 370-371, 2014.

[5] G. J. Hayes, Y. Liu, J. Genzer, G. Lazzi and M. D. Dickey, "Self-Folding Origami Microstrip," *IEEE Transactions on Antennas and Propagation*, vol. 62, no. 10, pp. 5416 - 5419, 2014.

[6] X. Liu, S. Georgakopoulos and M. Tentzeris, "A novel mode and frequency reconfigurable origami quadrifilar helical antenna," *2015 IEEE 16th Annual Wireless and Microwave Technology Conference (WAMICON)*, pp. 1-3, 2015.

[7] X. Liu, S. Yao, B. Cook, M. Tentzeris and S. Georgakopoulos, "An Origami Reconfigurable Axial-Mode Bifilar Helical Antenna," *IEEE Transactions on Antennas and Propagation,* vol. 63, no. 12, pp. 5897-5903, 2015.

[8] X. Liu, S. Yao, S. Georgakopoulos and M. Tentzeris, "Origami Quadrifilar Helix Antenna in UHF band," *2014 IEEE Antennas and Propagation Society International Symposium (APSURSI)*, pp. 372-373, 2014.

[9] Liu, Xueli, S. Yao and S. Georgakopoulos, "Reconfigurable spherical helical Electrically Small Antenna in UHF band," *2014 IEEE Antennas and Propagation Society International Symposium (APSURSI)*, pp. 368-369, 2014.

[10] S. R. Seiler, G. Bazzan, K. Fuchi, E. J. Alanyak, S. A. Gillman, G. W. Reich, P. R. Buskohl, S. Pallampati, D. Sessions, D. Grayson and G. H. Huff, "Physical Reconfiguration of an Origami-Inspired Deployable Microstrip Patch Antenna Array," *2017 IEEE International Symposium Antennas and Propagation & USNC/URSI National Radio Science Meeting*, pp. 2359-2360, 2017.

[11] S. Yao, X. Liu, S. Georgakopoulos and M. Tentzeris, "A novel reconfigurable origami spring antenna," *2014 IEEE Antennas and Propagation Society International Symposium (APSURSI)*, pp. 374-375, 2014.

[12] J. Hu, D. Pan and F. Dai, "Microstrip Patch Array Antenna With Reconfigurable Omnidirectional and Directional Patterns Using Bistable Composite Laminates," *IEEE ANTENNAS AND WIRELESS PROPAGATION LETTERS*, vol. 16, pp. 2485 - 2488, 2017.

[13] S. Mazlouman, A. Mahanfar and C. Menon, "Reconfigurable Axial-Mode Helix Antennas," *IEEE TRANSACTIONS ON ANTENNAS AND PROPAGATION*, vol. 59, no. 4, pp. 1070-1077, 2011.

[14] S. Yao, X. Liu and S. Georgakopoulos, "A mode reconfigurable Nojima origami antenna," *2015 IEEE International Symposium on Antennas and Propagation & USNC/URSI National Radio Science Meeting*, pp. 2237-2238, 2015.

[15] M. Schenk and S. Guest, "Geometry of Miura-folded metamaterials," *Proceedings of the National Academy of Sciences*, vol. 110, no. 9, pp. 3276-3281, 2013.

[16] S. Dabbak, H. Illias, B. Ang, N. Latiff and M. Makmud, "Electrical Properties of Polyethylene/Polypropylene Compounds for High-Voltage Insulation," *Energies*, vol. 11, no. 6, 2018.

[17] M. Nogi, N. Komoda, K. Otsuka and K. Suganuma, "Foldable nanopaper antennas for origami electronics," *Nanoscale*, no. 10, pp. 4395-4399, 2013.